nature medicine

# IL-23 induces spondyloarthropathy by acting on ROR-γt$^+$ CD3$^+$CD4$^-$CD8$^-$ entheseal resident T cells

Jonathan P Sherlock[1–3,5], Barbara Joyce-Shaikh[1,5], Scott P Turner[1], Cheng-Chi Chao[1], Manjiri Sathe[1], Jeff Grein[1], Daniel M Gorman[1], Edward P Bowman[1], Terrill K McClanahan[1], Jennifer H Yearley[1], Gérard Eberl[4], Christopher D Buckley[3], Robert A Kastelein[1], Robert H Pierce[1], Drake M LaFace[1,5] & Daniel J Cua[1,5]

**The spondyloarthropathies are a group of rheumatic diseases that are associated with inflammation at anatomically distal sites, particularly the tendon-bone attachments (entheses) and the aortic root. Serum concentrations of interleukin-23 (IL-23) are elevated and polymorphisms in the IL-23 receptor are associated with ankyosing spondylitis, however, it remains unclear whether IL-23 acts locally at the enthesis or distally on circulating cell populations. We show here that IL-23 is essential in enthesitis and acts on previously unidentified IL-23 receptor (IL-23R)$^+$, RAR-related orphan receptor γt (ROR-γt)$^+$CD3$^+$CD4$^-$CD8$^-$, stem cell antigen 1 (Sca1)$^+$ entheseal resident T cells. These cells allow entheses to respond to IL-23 *in vitro*—in the absence of further cellular recruitment—and to elaborate inflammatory mediators including IL-6, IL-17, IL-22 and chemokine (C-X-C motif) ligand 1 (CXCL1). Notably, the *in vivo* expression of IL-23 is sufficient to phenocopy the human disease, with the specific and characteristic development of enthesitis and entheseal new bone formation in the initial complete absence of synovitis. As in the human condition, inflammation also develops *in vivo* at the aortic root and valve, which are structurally similar to entheses. The presence of these entheseal resident cells and their production of IL-22, which activates signal transducer and activator of transcription 3 (STAT3)-dependent osteoblast-mediated bone remodeling, explains why dysregulation of IL-23 results in inflammation at this precise anatomical site.**



The spondyloarthropathies are a complex group of rheumatic diseases that are characterized by articular inflammation, erosion and new bone formation at peripheral and axial sites. Unlike rheumatoid arthritis, no therapies have been shown to be strongly disease modifying in the prototypical spondyloarthropathy, ankylosing spondylitis[1,2]. Although tumor necrosis factor (TNF) antagonism reduces the symptoms and spinal inflammation in ankylosing spondylitis[3,4], ultimately, new bone growth continues.

The primary articular site of inflammation in spondyloarthropathy has been proposed to be the enthesis[5], an anatomic region at the junction of tendon to bone, rather than the synovium. Although TNF overexpression in rodents has been used to model arthritis, these rodents develop a synovial-associated pathology with pannus formation that is more reminiscent of rheumatoid arthritis than spondyloarthropathy[6]. Despite the profound impact of TNF inhibition on the signs and symptoms of spondyloarthropathy, thus far, the evidence of its ability to affect the structural progression of the disorder is much weaker. Together, these findings suggest that pathways other than TNF are crucial in the development of the disease. It was noted recently that polymorphisms in the receptor for IL-23 are associated not only with ankylosing spondylitis but also with other associated conditions, such as psoriatic arthritis and inflammatory bowel disease[7–9]. Moreover, IL-23 is active at mucosal surfaces and is produced by the gut[10], suggesting that the intestinal mucosa could be a key site of IL-23 production in spondyloarthropathy, which is known to be associated with bowel inflammation secondary to autoimmune or infective processes. Indeed, intestinal inflammation and rheumatic pathology are closely linked[11]. Moreover human leukocyte antigen B27 (HLA-B27), which is present in up to 90% of patients with ankylosing spondylitis, has a tendency to misfold, and this misfolding results in the production of IL-23 (ref. 12). Moreover, IL-23 is also produced in response to the endoplasmic reticulum stress response that is triggered by *Chlamydia trachomatis*, a bacterium that is associated with the reactive arthritis subtype of spondyloarthropathy[13]. Taken together, these observations suggest that overproduction of, or heightened sensitivity to, IL-23 may be central to the pathogenesis of spondyloarthropathy. Indeed, serum concentrations of IL-23 are elevated in patients with ankylosing spondylitis[14–17].

It remains unclear how elevated IL-23 production is associated with inflammation specifically at the enthesis. It is now known that not only T helper type 17 ($T_H17$) cells but also a wide range of other immune cells can respond to IL-23 (ref. 18). Biopsies of entheseal lesions are extremely limited but show the presence of both macrophages and lymphocytes at this site[19–23]. Whether these entheseal cell populations can respond to IL-23 and, indeed, whether IL-23 acts locally at the enthesis or distally on circulating populations is unknown.

We show here that IL-23 promotes highly specific entheseal inflammation by acting on a previously unidentified population of CD3$^+$CD4$^-$CD8$^-$ entheseal resident lymphocytes and also

[1]Merck Research Laboratories, Palo Alto, California, USA. [2]University of Oxford, Trinity College, Oxford, UK. [3]University of Birmingham, Birmingham, UK. [4]Institut Pasteur, Paris, France. [5]These authors contributed equally to this work. Correspondence should be addressed to D.J.C. (daniel.cua@merck.com).

Received 14 November 2011; accepted 27 April 2012; published online 1 July 2012; doi:10.1038/nm.2817

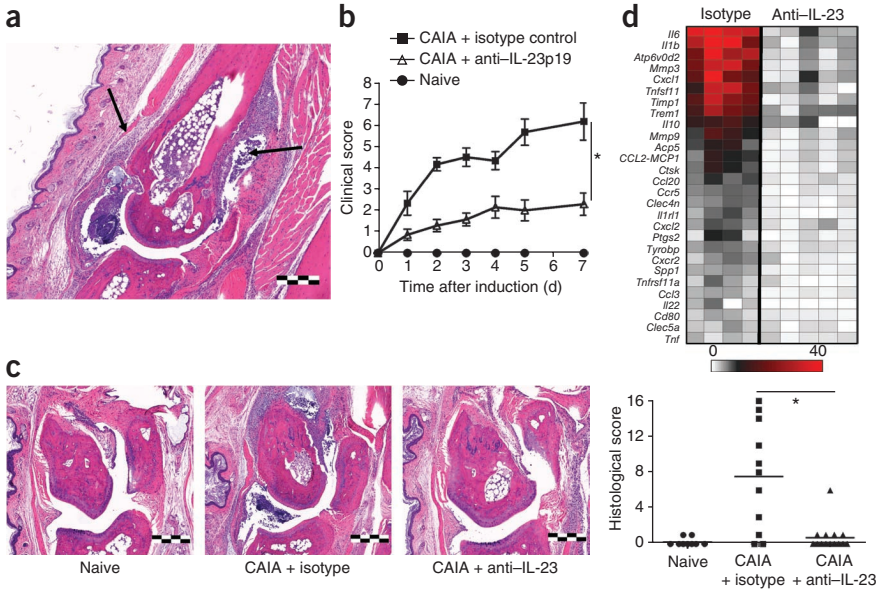


**Figure 1** Entheseal inflammation in a passive transfer model of collagen-antibody–induced arthritis (CAIA) is dependent on IL-23. (**a**) Paw histology 7 d after type II–collagen–specific antibody transfer in B10.RIII male mice. Arrows indicate entheseal inflammation. Scale bar, 500 μm. The stain used was H&E. (**b**) Clinical scores of mice with CAIA in the presence of neutralizing antibody to IL-23p19 (anti–IL-23p19) and isotype control antibodies. $^*P = 0.025$ by Mann Whitney test. The graph shows the means and s.e.m., with seven mice per group. (**c**) Histology performed on the same treatment groups in **b** at day 7 after antibody transfer and histological enthesitis score. Scale bars, 500 μm. The stain used was H&E. $^*P = 0.0023$ by Mann Whitney test. (**d**) Molecular profiling by quantitative PCR on individual mice from the same treatment groups. The colored bar shows the fold upregulation of gene expression in comparison to naive mice. Data are representative of three independent experiments.

that expression of this cytokine alone, in the absence of any other inflammatory signal, is sufficient to reproduce the classical systemic features of spondyloarthropathy.

## RESULTS

### IL-23 drives enthesitis *in vivo*

We sought to investigate the role of IL-23 in joint inflammation. The arthritis model induced by type II–collagen–specific antibodies is characterized by broad articular inflammation and synovitis, however, we noted that on day 7 after passive immunization, B10.RIII mice also developed severe enthesitis. Indeed, this enthesitis was prominent before progression to the well-defined destructive arthritis of the articular surfaces (**Fig. 1a**).

Neutralization with an antibody to the IL-23 subunit p19 (IL-23p19) given at disease induction not only reduced clinical disease scores (**Fig. 1b**) but also reduced histological entheseal inflammation (**Fig. 1c**). This reduction was associated with the downregulation of several inflammatory mediators, such as *Il6* and *Il1b*, and genes known to be involved in erosion of bone and tissue, such as *Rankl*, *Ctsk* and matrix metalloproteinases (**Fig. 1d**). Chemokines, including those encoded by *Cxcl1* and *Cxcl2*, are likewise downregulated. The entheseal inflammation observed is consistent with the presence of type II collagen in entheseal fibrocartilage[24–32], with its specific localization in fibrocartilage but not in the tendon proper[28,32], and the ability of immunization with type II collagen to induce an ossifying enthesopathy in rats[33]. We thus sought to investigate the role of IL-23 in enthesitis.

### Entheses contain an IL-23R$^+$ resident cell

Although the association between SNPs in the IL-23R and clinical spondyloarthropathy is now well established, the key site of action of

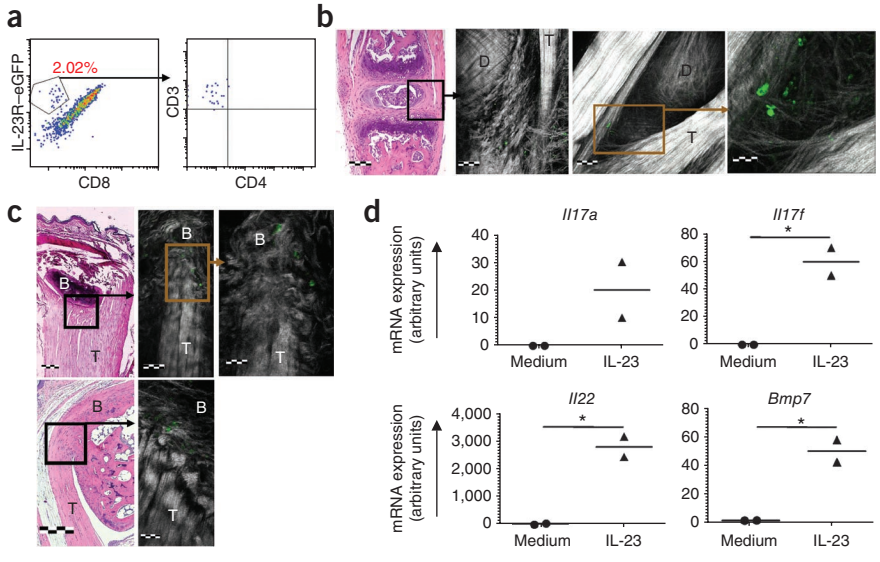


**Figure 2** Entheses contain an IL-23R$^+$ resident cell population. (**a**) Flow cytometry of entheseal cell suspensions from naive IL-23R–eGFP reporter mice. The initial plot (left) was gated on CD45$^+$ entheseal cells, the second plot (right) was gated on GFP$^+$ cells. (**b**) Multiphoton microscopy of naive, intact axial tissue from IL-23R–eGFP reporter mice. A representative H&E section (left, scale bar, 200 μm) is included to show the anatomical site of the multiphoton image (center left, scale bar, 50 μm). Fine entheseal fibers are visible in relation to the longitudinal tendon (T) and intervertebral disc (D). Collagen is shown in white, and GFP is shown in green. The center right image (scale bar, 50 μm) shows another example, with an enlarged image shown on the right (scale bar, 20 μm). (**c**) Multiphoton microscopy of Achilles' tendon and entheses from an intact heal from naive IL-23R–eGFP mice. A posterior view (top) and lateral view (bottom) are shown, with representative H&E sections (upper left, scale bar, 200 μm; lower left, scale bar, 100 μm) showing the anatomical locations. The image on the upper right (scale bar, 20 μm) is an enlargement of the upper middle image (scale bar, 40 μm). T, Achilles' tendon; B, bone (calcaneum). Collagen is shown in white, and GFP is shown in green. Lower right, scale bar, 20 μm. (**d**) Effects of IL-23 on gene expression in Achilles' entheses after overnight *in vitro* organ culture compared with control medium. Pooled entheses from ten mice were used for each data point. $^*P < 0.01$ by *t* test. Data are representative of more than five independent experiments (**a**–**c**) or three independent experiments (**d**).

IL-23 in spondyloarthropathy has remained elusive. IL-23–responsive cells are located at sites such as mucosal surfaces, where they are crucial in the maintenance of tissue homeostasis and barrier function[18]. Entheses show histological features of continual tissue damage and repair[34], and we hypothesized that entheses themselves contain IL-23R$^+$ cells that are capable of responding locally to IL-23 and inducing inflammation and remodeling. We used IL-23R–eGFP reporter mice to investigate the presence of such cells.

An evaluation of CD45$^+$ entheseal cells from naive mice using flow cytometry revealed that the IL-23R–eGFP$^+$ fraction expresses CD3 but is double negative (DN) for CD4 and CD8 (**Fig. 2a**). To show the exact anatomical location of these cells, we performed multiphoton

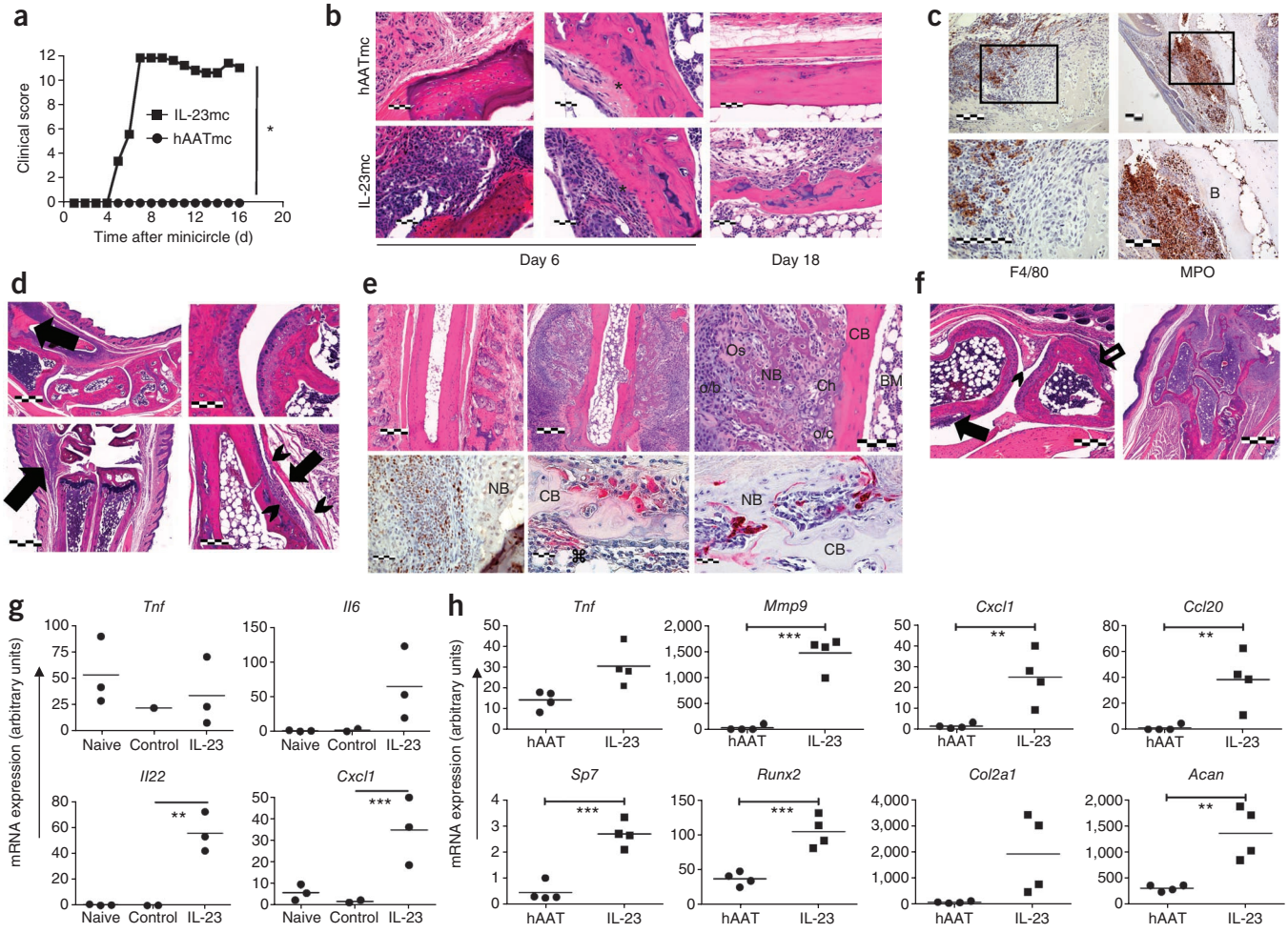


**Figure 3** Systemic IL-23 expression *in vivo* induces highly specific entheseal inflammation. (**a**) Clinical paw swelling scores in B10.RIII mice treated with 3 μg IL-23mc or human α1 anti-trypsin control minicircle (hAATmc). $^*P < 0.001$ by Mann Whitney test. (**b**) Two examples of entheseal histology at day 6 after IL-23mc or control hAATmc treatment (scale bars, 40 μm) and histology of periosteal disease and osteoblast expansion at day 18 after treatment (scale bars, 50 μm) in B10.RIII mice. The asterisks indicate the entheseal tendon-bone interface. (**c**) Immunoperoxidase staining of the entheseal infiltrate for MPO and F4/80 after 18 days of *in vivo* IL-23 expression. Bone (B) is marked, and the counterstain used was hematoxylin. The bottom row of images shows magnified views of the boxed areas in the upper images. Scale bars, 200 μm. (**d**) Entheseal histology at day 35 after treatment (upper left, scale bar, 500 μm), with new entheseal bone formation indicated (arrow). To the right is a magnified view of the normal articular surface at 35 d after treatment (upper right, scale bar, 100 μm). Early enthesitis of carpal entheses (arrow) at day 8 after treatment (lower left, scale bar, 500 μm). The specificity of IL-23–induced enthesitis at day 8 after treatment is shown in relation to the tendon approaching and connecting to the bone (arrowheads) compared to the intervening tendon (arrow) (lower right, scale bar, 500 μm). (**e**) Periosteal bone formation 18 d after IL-23mc administration (upper middle, scale bar, 400 μm) compared with control hAATmc treatment (upper left, scale bar, 400 μm). The image on the upper right is a magnified view (scale bar, 50 μm) showing the relation of chondrocyte-rich cartilage (Ch), new bone (NB), osteoid (Os), osteoblasts (o/b) and osteoclasts (o/c) to cortical bone (CB) and bone marrow (BM). The image on the lower left shows a Ki-67 immunoperoxidase stain of proliferating cells with a hematoxylin counterstain (scale bar, 50 μm), the image in the lower middle shows osteoblasts stained for alkaline phosphatase, and the image on the lower right shows osteoclasts stained for tartrate-resistant alkaline phosphatase (scale bars, 20 μm). (**f**) Enthesitis (open arrow) and periostitis (filled arrow) at day 35 after treatment (left, scale bar, 500 μm) showing continuity of the enthesis and synovium (arrowhead), with erosive disease at day 67 after treatment (right, scale bar, 800 μm). Data are representative of three similar experiments (**a**–**f**). (**g**) Molecular profiling of microdissected entheses after 5 d of systemic expression of IL-23 compared to treatment with control (albumin) minicircle or to naive tissue. $^{**}P = 0.01$, $^{***}P = 0.006$ by *t* test. Each data point represents pooled Achilles' entheses from four B10.RIII mice. (**h**) Molecular profiling of microdissected Achilles' entheses after 4 weeks of IL-23 expression *in vivo* compared to hAAT control treatment. Each data point shows one of four repeats of the results from 14 Achilles' entheses from seven mice; the bar indicates the mean. $^*P < 0.05$, $^{**}P < 0.006$, $^{***}P < 0.001$ by *t* test.

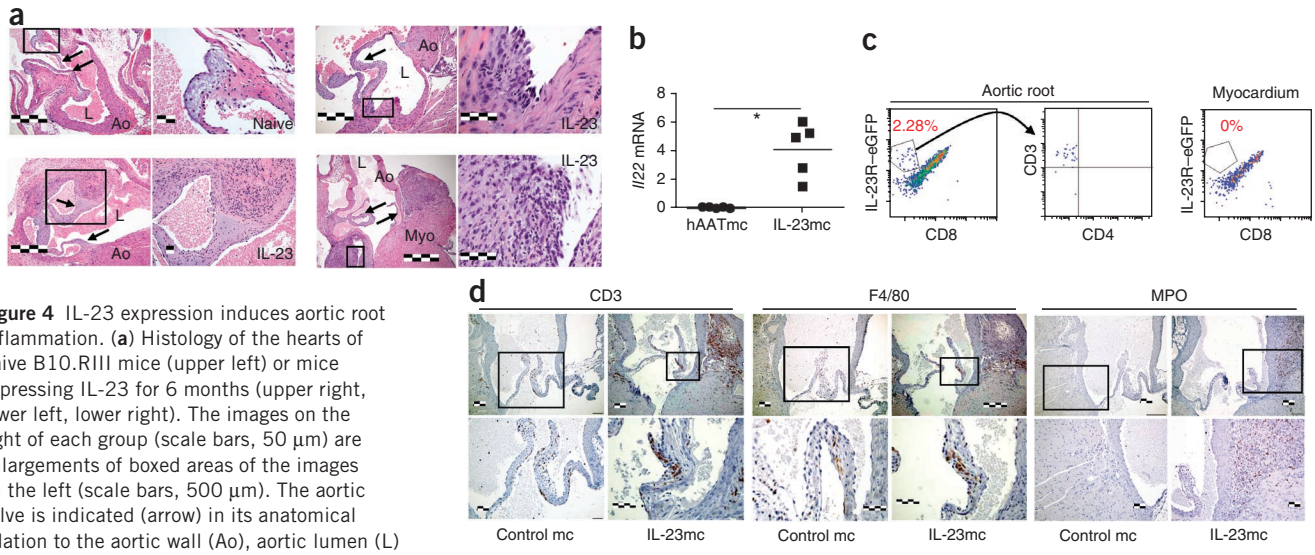


**Figure 4** IL-23 expression induces aortic root inflammation. (**a**) Histology of the hearts of naive B10.RIII mice (upper left) or mice expressing IL-23 for 6 months (upper right, lower left, lower right). The images on the right of each group (scale bars, 50 μm) are enlargements of boxed areas of the images on the left (scale bars, 500 μm). The aortic valve is indicated (arrow) in its anatomical relation to the aortic wall (Ao), aortic lumen (L) and myocardium (Myo). Data are representative of three independent experiments. (**b**) Molecular profiling of the aortic root after treatment with IL-23mc or control hAATmc. Each data point represents one of five separate isolated aortic roots. $^*P = 0.0013$ by *t* test. (**c**) Flow cytometric evaluation of cell suspensions prepared from the aortic root and valve or the myocardium of naive IL-23R–eGFP reporter mice. The initial plot (left) was gated on CD45$^+$ cells. (**d**) Immunohistochemical staining of aortic roots 2 months after administration of IL-23mc or control (mutated, inactive IL-23) minicircle (control mc). Data are representative of the stained hearts of more than five mice. The images in the bottom row (scale bars, 50 μm) are magnified views of the boxed areas in the images in the top row (scale bars, 100 μm).





microscopy on intact, live, unmanipulated tissue from naive mice. We found that IL-23R–eGFP$^+$ cells are located at the entheseal interface between the tendon and bone at both axial (**Fig. 2b**) and peripheral (**Fig. 2c**) articular locations and that these cells are absent from the tendon proper.

To confirm the direct responsiveness of entheses to IL-23 in the absence of further cellular infiltration, we cultured entheseal tissue by incubation at an air-liquid interface. Entheses in culture respond to IL-23 by upregulating expression of *Il17a, Il17f*, *Il22* and bone morphogenic protein 7 (*Bmp7*) (**Fig. 2d**).

### IL-23 alone is sufficient to drive enthesitis *in vivo*

Given the presence of IL-23R$^+$ entheseal resident cells, we next investigated the effects of the expression of IL-23 on entheses *in vivo*. Because IL-23 transgenic mice die at a young age[35], we used minicircle DNA technology[36] to express IL-23 in the hepatocytes of mice. Hydrodynamic delivery of an IL-23 minicircle (IL-23mc) into the tail veins of mice resulted in long-term expression of IL-23 and elevated serum IL-23 concentration for 100 d, with a titratable dose response (**Supplementary Fig. 1**).

After systemic expression of IL-23 resulting from the administration of IL-23mc, B10.RIII mice developed severe paw swelling (**Fig. 3a**), with the severity of the swelling correlating with the dose of IL-23mc (**Supplementary Fig. 1**). At the highest dose, mice developed clinical disease 5 d after administration, with the maximal disease score being attained by day 7–10 after administration (**Fig. 3a**). Despite this rheumatic pathology in B10.RIII mice, there was no histopathological disease in the gut, liver and kidney of the mice, even at 100 d after administration (data not shown). An examination of early disease showed that the inflammatory pathology is focused on the entheses and periosteum, with severe entheseal inflammation developing at 6 d after induction of IL-23 expression and expansion of periosteal osteoblasts developing by day 18 (**Fig. 3b**). The entheseal infiltrate is composed of F4/80$^+$ macrophages and myeloperoxidase (MPO)$^+$ neutrophils (**Fig. 3c**). A histological analysis after 35 d of IL-23 exposure revealed the highly specific presence of enthesitis in the entheses of both the front and back paws and, crucially, such enthesitis was present in the absence of synovial joint destruction at this time point (**Fig. 3d**).

An examination of the articular structures in the mice showed the presence of new entheseal bone after 18 d of elevated systemic IL-23 expression (**Fig. 3e**). We also found formation of cartilage, osteoid and new bone at the periosteum, along with osteoblasts and chondrocytes, and Ki-67 staining demonstrating active proliferation at this site. Moreover, we found multinucleate osteoclasts to be eroding the cortical bone, showing both the anabolic and catabolic bone changes that are characteristic of spondyloarthropathy (**Fig. 3e**). Although early disease is characterized by specific entheseal inflammation, at later time points, synovitis with destruction of the articular surfaces is evident in association with florid enthesitis (**Fig. 3f**). *Ex vivo* molecular profiling of microdissected entheseal tissue showed the induction of *Il6*, *Il22* and *Cxcl1* by day 5 of IL-23 expression compared to naive mice and those receiving a control minicircle (**Fig. 3g**). After 4 weeks of IL-23 expression *in vivo*, the upregulation of genes involved in the recruitment of neutrophils (*Cxcl1*) and the induction of a bone remodeling program were evident in entheses isolated *ex vivo* (**Fig. 3h**), as evidenced by upregulation of *Col2a* and *Acan* and induction of *Runx2* and *Sp7*, genes that regulate the differentiation of osteoblasts and chondrocytes. The upregulation of *Ccl20* at this time point shows the potential for the inflamed enthesis to recruit additional IL-23–responsive cells. Despite their upregulation, IL-23–driven disease is not substantially ameliorated by the neutralization of TNF, IL-6 or receptor activator of nuclear factor κB ligand (RANKL) (**Supplementary Fig. 2**).

Examination of the spines of the treated mice revealed the presence of axial enthesitis at the sites of attachment of the spinal ligaments to bone and sacroiliitis (**Supplementary Fig. 3**) after *in vivo* IL-23 exposure. Psoriasis was also present in mice expressing IL-23 (**Supplementary Fig. 3**).

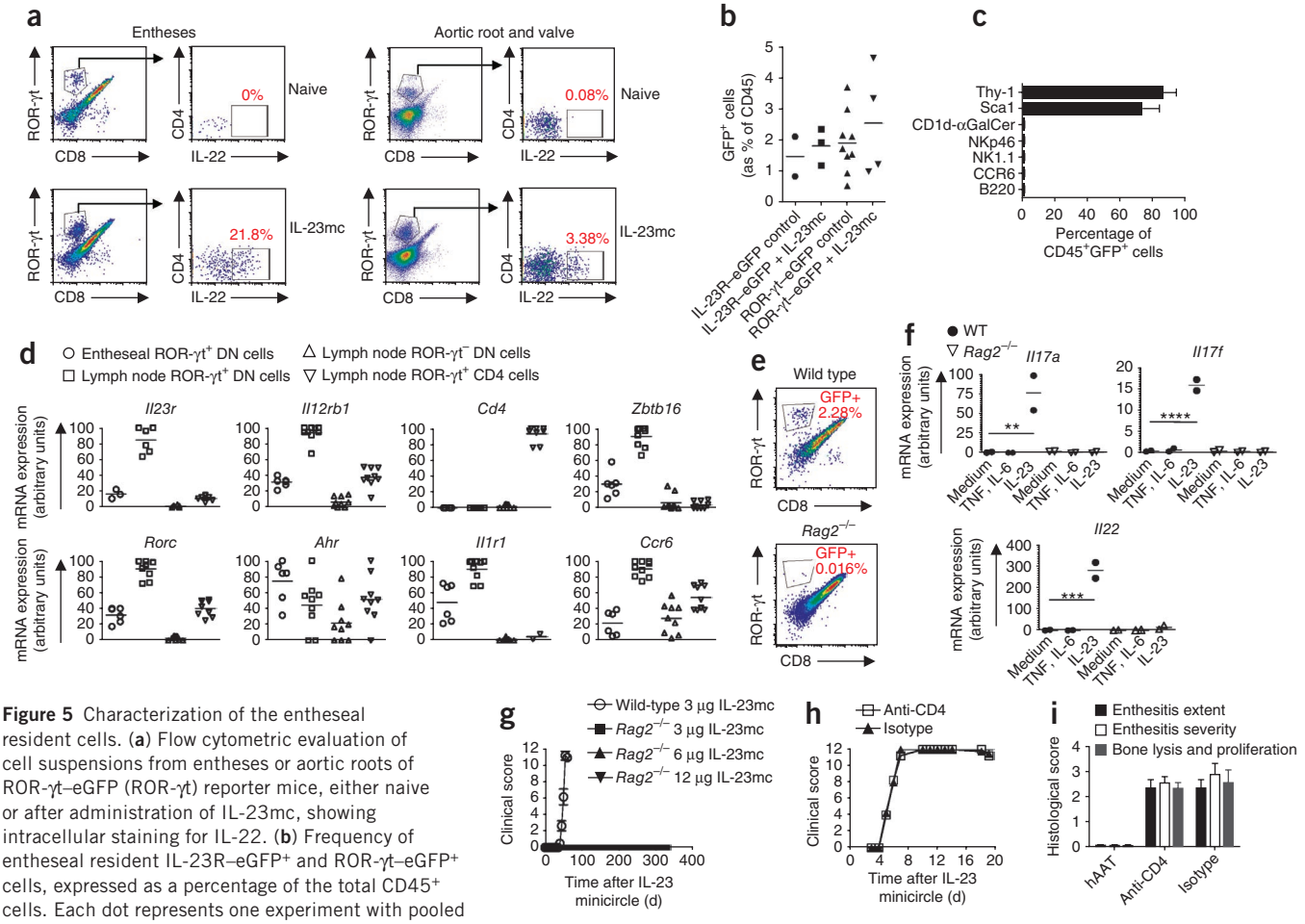


**Figure 5** Characterization of the entheseal resident cells. (**a**) Flow cytometric evaluation of cell suspensions from entheses or aortic roots of ROR-γt–eGFP (ROR-γt) reporter mice, either naive or after administration of IL-23mc, showing intracellular staining for IL-22. (**b**) Frequency of entheseal resident IL-23R–eGFP$^+$ and ROR-γt–eGFP$^+$ cells, expressed as a percentage of the total CD45$^+$ cells. Each dot represents one experiment with pooled entheses from two mice. (**c**) Immunophenotype of ROR-γt–eGFP$^+$ cells from naive mice, expressed as a percentage of the total CD45$^+$GFP$^+$ entheseal cells. Data are pooled from three independent experiments. Bars show the mean and s.e.m. CD1d-αGalCer, α-galactosylceramide–loaded CD1d tetramer. (**d**) Molecular profiling of sorted naive ROR-γt$^+$ entheseal CD4$^-$CD8$^-$ (DN) T cells compared with populations of lymph node cells. Data are pooled from three independent experiments. Each data point represents a PCR analysis performed on 20–30 sorted cells, with the maximum expression normalized to 100. The bars represent the mean. (**e**) Flow cytometric analysis of dissociated entheseal cells from ROR-γt–eGFP reporter mice on a wild-type or *Rag2*$^{-/-}$ background. Each plot represents pooled samples from three mice. Data are representative of two independent experiments. (**f**) Inflammatory cytokine expression in isolated wild-type (WT) or *Rag2*$^{-/-}$ entheses cultured *in vitro* overnight with TNF and IL-6 or with IL-23. Each dot represents peripheral paw entheses pooled from ten mice. Data are representative of three independent experiments. $^{**}P < 0.05$, $^{***}P < 0.01$, $^{****}P < 0.005$ by *t* test. (**g**) Clinical paw swelling scores of wild-type or *Rag2*$^{-/-}$ C57BL/6 mice treated with IL-23mc. Wild-type mice were euthanized after maximal disease induction. (**h**) Clinical paw swelling score of B10.RIII mice treated with IL-23mc in the presence of depleting antibody to CD4 (anti-CD4) or isotype control antibody. $P = 0.90$ by Mann Whitney test for comparison of the terminal scores. (**i**) Histological enthesitis score in mice treated with control hAATmc or IL-23mc in the presence of either depleting antibody to CD4 or isotype control antibody from day −1. Data are representative of three independent experiments and are shown as mean with s.e.m. (**g**–**i**).

### IL-23R$^+$CD4$^-$CD8$^-$T cells reside in the aortic root

Spondyloarthropathy in humans is associated with inflammation of the aortic root and proximal aorta, leading to aortic valve insufficiency[37]. We therefore examined the hearts of mice expressing IL-23 *in vivo*, and we found that in contrast to naive mice, mice overexpressing IL-23 developed inflammation of the attachment site of the aorta valve to the aortic wall (**Fig. 4a**). A range of lesions were present that showed early inflammation of the point of valve insertion, increased inflammation of this insertion site and extensive inflammation of the aortic root without inflammation of the myocardium. A molecular analysis showed the induction of *Il22* expression in the aortic root after IL-23 exposure *in vivo* compared to mice treated with a control minicircle (**Fig. 4b**).

The aortic valve and peripheral entheses are known to have histological similarities, including the presence of cartilage and chondrocytes where the valve joins the aorta proper and where the valve moves and flexes like an entheses. We hypothesized that the aortic valve and root might contain similar cells to peripheral entheses. Indeed, a flow cytometric analysis showed the presence of IL-23R$^+$CD4$^-$CD8$^-$ T cells in the aortic root and valve but not in the myocardium (**Fig. 4c**), which is consistent with the histological evidence of pathology at this site after IL-23mc administration. Overexpression of IL-23 resulted in a dense infiltrate of T cells, macrophages and neutrophils in the aortic root (**Fig. 4d**).

### IL-23 promotes IL-17 and IL-22 expression by entheseal cells

Because ROR-γt is a key transcription factor in IL-23–responsive cells[38], we sought to determine whether our cell population of interest expresses this transcription factor. We therefore prepared cell

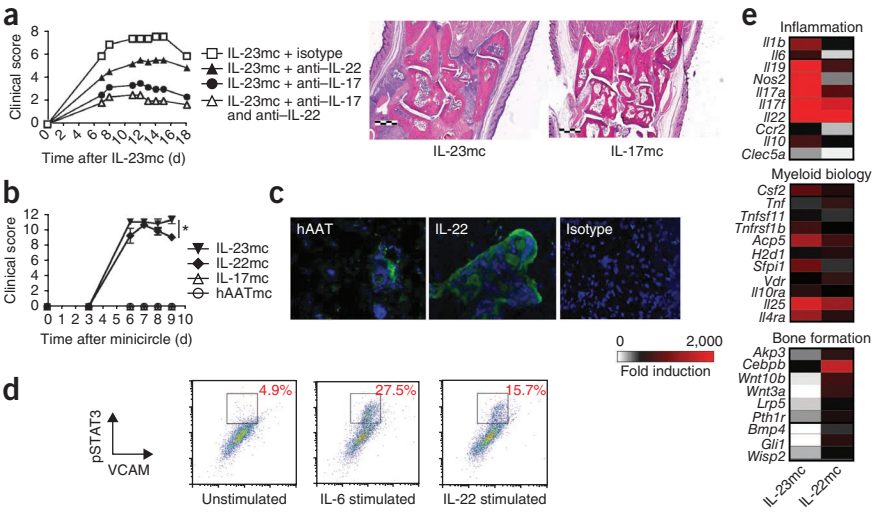


**Figure 6** IL-22 induces a bone remodeling program. (**a**) Clinical paw swelling score during IL-23mc–induced disease in B10.RIII mice in the presence of a neutralizing antibody to IL-22, a neutralizing antibody to IL-17 or both antibodies (left). Data points represent the mean of six mice. Shown are the histology of the paws of the mice 18 d after administration of IL-23mc or IL-17mc (middle and right images, scale bars, 500 μm). (**b**) Clinical score after administration of minicircles encoding a range of inflammatory cytokines. $^*P = 0.20$ by Mann Whitney test. Data points show the mean of five mice per group. (**c**) Immunofluorescent microscopy of phosphorylated STAT3 (pSTAT3) in paws to show the effects of prior exposure to IL-22 or control (hAAT). Isotype staining is shown, with pSTAT3 in green and DAPI in blue. (**d**) Assessment of pSTAT3 by flow cytometry of the osteoblast cell line CRL-12424 without stimulation or after stimulation with IL-6 or IL-22. (**e**) Molecular profiling of gene expression in paws 20 d after administration of IL-22mc or IL-23mc. The colored bar shows the fold upregulation in comparison to mice treated with control minicircle. Data are representative of three (**a**–**c**) or two (**d**,**e**) independent experiments.





suspensions from entheses and aortic roots of ROR-γt–eGFP reporter mice and identified the presence of ROR-γt$^+$ entheseal T cells, which are also double negative for CD4 and CD8 (**Fig. 5a**,**b**).

We next examined the effects of IL-23–mediated activation of these cells *in vivo*. We treated mice with IL-23mc, and we isolated their entheseal cells 8 d after the onset of clinical disease and examined them for cytokine expression. ROR-γt$^+$CD4$^-$CD8$^-$ entheseal T cells from mice with systemic IL-23 expression, but not those from naive mice, expressed intracellular IL-22 protein when treated *ex vivo* with phorbol myristate acetate and ionomycin (**Fig. 5a**). An examination of the resident cells of the aortic root of the IL-23mc–treated mice revealed that the ROR-γt$^+$CD4$^-$CD8$^-$ cells also produced IL-22 after exposure to IL-23 *in vivo* (**Fig. 5a**). Pooled results from multiple experiments revealed that IL-23R$^+$ and ROR-γt$^+$ entheseal resident cells were present at a frequency on the order of 2% of the entheseal CD45$^+$ hematopoietic cells (**Fig. 5b**). The IL-23R$^+$ and ROR-γt$^+$ cells express thymus cell antigen 1 (Thy-1) and Sca1 but not natural cytotoxicity triggering receptor 1 (NKp46) or killer cell lectin-like receptor subfamily B member 1C (NK1.1), and they do not bind α-galactosylceramide–loaded CD1d tetramers (**Fig. 5c**). To further characterize these cells, we performed molecular profiling of sorted entheseal resident ROR-γt–eGFP$^+$CD4$^-$CD8$^-$ T cells, and we compared these cells with ROR-γt–eGFP$^+$ and ROR-γt–eGFP$^-$CD4$^-$CD8$^-$ T cells and ROR-γt–eGFP$^+$CD4$^+$ cells from the inguinal lymph nodes (**Fig. 5d**). The expected distribution of the expression of *Il23r*, *Il12rb1* and *Rorc* in the ROR-γt$^+$ cells and of *Cd4* in the CD4$^+$ cells confirmed the purity of the cell sorting. This analysis reveals that the ROR-γt$^+$CD4$^-$CD8$^-$ T cells express *Il1r1* and *Ahr*, which is consistent with findings in other IL-23–responsive cell types. We show that these CD4$^-$CD8$^-$ T cells also express *Zbtb16*, which encodes the PLZF transcription factor that allows cells to respond immediately to cytokines. Consistent with their tissue resident status, the entheseal ROR-γt$^+$CD4$^-$CD8$^-$ T cells do not express *Ccr6*.

## Enthesitis requires a *Rag*-dependent cell but not $T_H17$ cells

We next sought to confirm the role of the entheseal resident CD4$^-$CD8$^-$ T cell population by examination of *Rag2*$^{-/-}$ mice. Crossing ROR-γt–eGFP C57BL/6 reporter mice with *Rag2*$^{-/-}$ mice confirmed that, in contrast to the ROR-γt–eGFP$^+$ entheseal resident cells we found in wild-type mice, *Rag2*$^{-/-}$ mice do not have this cell population (**Fig. 5e**). The presence of CD4$^-$CD8$^-$ T cells is required for entheseal responsiveness to IL-23, as *Rag2*$^{-/-}$ entheses do not upregulate cytokines in response to *in vitro* stimulation with IL-23, whereas wild-type entheses upregulate *Il17a*, *Il17f* and *Il22* after this treatment (**Fig. 5f**). Development of entheseal inflammation is similarly abrogated *in vivo* in C57BL/6 *Rag2*$^{-/-}$ mice, which do not develop disease despite confirmed high expression of IL-23 serum protein for 1 year after injection of IL-23mc, whereas C57BL/6 wild-type mice develop disease by 45–50 d after exposure (**Fig. 5g**). These *Rag2*$^{-/-}$ mice expressing IL-23 have normal paw histology (data not shown).

As $T_H17$ cells are crucial in many IL-23–dependent inflammatory disorders, we sought to investigate the role of these cells in IL-23–driven enthesitis. We depleted $T_H17$ cells in wild-type B10.RIII mice with an antibody specific to CD4 and found that this did not alter the course of clinical disease after administration of IL-23mc (**Fig. 5h**). Moreover, the histological enthesitis score was not reduced by depletion of CD4$^+$ cells (**Fig. 5i**). We confirmed depletion by the antibodies to CD4 by showing an absence of CD4$^+$ cells in the lymph nodes (**Supplementary Fig. 4**). Moreover, we found that CD4$^+$ cells are not present in the enthesis during clinical disease at day 10 after IL-23mc administration (**Supplementary Fig. 4**). These findings confirm that disease is independent of $T_H17$ cells, which is consistent with the key role of the local resident IL-23R$^+$ entheseal cell population in mediating disease.

## IL-22 promotes entheseal and periosteal bone formation

IL-23 is an immunomodulatory cytokine, the effects of which are mediated by downstream cytokines such as IL-17 and IL-22. Indeed, we found that entheseal resident cells produce IL-17 (**Supplementary Fig. 5a**) and IL-22 (**Fig. 5a**) after *in vivo* stimulation with IL-23. To assess the role of these cytokines, we administered neutralizing antibodies to IL-17, neutralizing antibodies to IL-22 or both antibodies after inducing IL-23–mediated enthesitis in B10.RIII mice by IL-23mc administration. Inhibition of IL-17 or IL-22 resulted in decreased clinical paw swelling scores, particularly when the two antibodies were administered together (**Fig. 6a**). Overexpression of IL-17 using minicircle technology, however, did not lead to clinical or histological pathology (**Fig. 6a**,**b**).

We next tested whether IL-22 could act on bone cells and mediate the osteoproliferative effects observed after expression of IL-23. To examine the effects of IL-22 on entheseal bone growth, we induced systemic expression of IL-22 in B10.RIII mice using a minicircle DNA vector specific for IL-22 and, as for IL-23, this resulted in clinically evident paw swelling (**Fig. 6b**). Immunofluorescence revealed increased phosphorylation of STAT3 that was localized to the bone (**Fig. 6c**). Osteoblasts are central to the formation of new bone, and, using the osteoblast cell line CRL-12424, we found that IL-22 can induce phosphorylation of STAT3 in these cells (**Fig. 6d**). Although *in vivo* expression of IL-23 is more effective than expression of IL-22 in upregulating inflammatory genes in the paws of mice, IL-22 more effectively induces genes that regulate bone formation, specifically those that encode Wnt family members, bone morphogenic proteins and alkaline phosphatase (**Fig. 6e**). Taken together, these results suggest that the osteoproliferative component of disease is mediated by IL-22.

## DISCUSSION

Although certain diseases are associated with clear evidence of autoreactivity, other inflammatory conditions can result from mutations that cause elevated cytokine signaling[39]. Despite the strong and robust association of HLA-B27 with ankylosing spondylitis[12], no reproducible evidence for an antigen-specific response in this disease has emerged. Indeed, spondyloarthropathy in HLA-B27 transgenic rodents is not associated with the activation of CD8 T cells[40] and is independent of these lymphocytes[40,41]. The precise anatomical pattern of pathology seems inconsistent with a pattern determined only by antigen reactivity[42].

Recent findings have converged on the cytokine IL-23 as a key factor in spondyloarthropathy. HLA-B27 can misfold, triggering a cellular stress response resulting in the production of IL-23 (ref. 12), and polymorphisms in IL-23R are associated with ankylosing spondylitis and its associated conditions[8,9,43]. It remains unclear how such elevated IL-23 production can result in the distinct pattern of inflammatory involvement observed in spondyloarthropathy.

We show here that the anatomical sites that are inflamed in spondyloarthropathy are primed to rapidly react to IL-23 by the presence of a previously unidentified population of IL-23R$^+$ resident cells that express the PLZF transcription factor, which is known to confer an immediate, 'innate-like' responsiveness[44]. *In vivo* exposure to IL-23 is sufficient to induce highly specific entheseal inflammation in the absence of $T_H17$ cells and with rapid kinetics. The enthesis is therefore a functional IL-23–responsive anatomic site that, like the gut and lung, which contain innate IL-23–responsive cells[18], is primed to respond immediately to IL-23.

CD4$^-$CD8$^-$ T cells are also central to the lupus-like disease seen in MRL/*lpr* mice[45], and IL-23R controls the expansion and elaboration of IL-17 by CD4$^-$CD8$^-$ T cells in wild-type mice during infection[46], where at early stages they contribute more to IL-17 production than do conventional $T_H17$ cells[47]. CD4$^-$CD8$^-$ T cells are also found in humans with lupus[48] and have been associated with Behcet's disease[49,50] and systemic sclerosis[51]. Together with our finding of their central role in IL-23–mediated spondyloarthropathy, this shows the key role of these double-negative cells more broadly in the rheumatic inflammation of connective tissue.

Our experimental model of systemic IL-23 overexpression is relevant to the spondyloarthropathies, as these diseases are accompanied by elevated concentrations of serum IL-23 (refs. 14–17). The relationship between intestinal inflammatory disease and rheumatic symptoms[11] suggests that circulating gut-derived IL-23 may be responsible for the rheumatic inflammation. Indeed, ankylosing spondylitis is associated with elevated expression of IL-23 in the intestine[15].

We propose that the various systemic manifestations of spondyloarthropathy represent a fundamental unity: genetically, the various subtypes share common susceptibility genes, and they are intimately interrelated clinically; immunologically, they have dysregulated IL-23 biology in common. We suggest that neutralization of IL-23 pathway targets, including IL-17 and IL-22, may ameliorate disease pathology at the various anatomical sites that are inflamed in spondyloarthropathy and that these are promising targets for the treatment of ankylosing spondylitis.

## METHODS

Methods and any associated references are available in the online version of the paper.

*Note: Supplementary information is available in the online version of the paper.*

### ACKNOWLEDGMENTS

We are grateful for the assistance of S. Jungers for flow cytometric sorting. We also thank P. Bowness, H. Gaston, A. van der Merwe and A. Cooke for helpful comments on this study. This research was funded by and conducted within Merck Research Laboratories. We thank Z.-Y. Chen (Departments of Pediatrics and Genetics, Stanford University School of Medicine) for the minicircle vector plasmid.

### AUTHOR CONTRIBUTIONS

J.P.S. identified the role of IL-23 in enthesitis, designed and performed the experiments to investigate IL-23 induction of rheumatic lesions, developed the methodology to isolate, culture and analyze entheseal cells and prepared the manuscript. B.J.-S. identified the role of IL-22 in entheseal disease and designed and performed IL-22 signaling and antibody blocking studies, as well as studies using antibodies against collagen to induce arthritis. S.P.T. directed and performed the multiphoton microscopy and assisted with flow cytometry. C.-C.C., E.P.B. and C.D.B. provided expert advice about murine arthritis models. M.S., J.G. and T.K.M. provided the gene expression data. D.M.G. produced, validated and provided all gene expression minicircle constructs. J.H.Y. and R.H.P. directed histological studies and analyses and developed an enthesitis scoring system. G.E. provided ROR-γt–eGFP reporter mice and discussed key experimental designs. R.A.K. provided expert advice to enable the IL-23 minicircle project. D.M.L. supervised the project and performed the hydrodynamic injections. D.J.C. directed the project, oversaw the experimental design, data analysis and research direction and prepared the manuscript.

### COMPETING FINANCIAL INTERESTS

The authors declare competing financial interests: details are available in the online version of the paper.

Published online at http://www.nature.com/doifinder/10.1038/nm.2817.
Reprints and permissions information is available online at http://www.nature.com/reprints/index.html.

1. Lories, R.J., de Vlam, K. & Luyten, F.P. Are current available therapies disease-modifying in spondyloarthritis? *Best Pract. Res. Clin. Rheumatol.* **24**, 625–635 (2010).
2. Maksymowych, W.P. Disease modification in ankylosing spondylitis. *Nat. Rev. Rheumatol.* **6**, 75–81 (2010).
3. Lambert, R.G. *et al.* Adalimumab significantly reduces both spinal and sacroiliac joint inflammation in patients with ankylosing spondylitis: a multicenter, randomized, double-blind, placebo-controlled study. *Arthritis Rheum.* **56**, 4005–4014 (2007).
4. van der Heijde, D. *et al.* Assessment of radiographic progression in the spines of patients with ankylosing spondylitis treated with adalimumab for up to 2 years. *Arthritis Res. Ther.* **11**, R127 (2009).
5. McGonagle, D., Gibbon, W. & Emery, P. Classification of inflammatory arthritis by enthesitis. *Lancet* **352**, 1137–1140 (1998).
6. Keffer, J. *et al.* Transgenic mice expressing human tumour necrosis factor: a predictive genetic model of arthritis. *EMBO J.* **10**, 4025–4031 (1991).
7. Rahman, P. *et al.* Association of interleukin 23 receptor variants with psoriatic arthritis. *J. Rheumatol.* **36**, 137–140 (2009).
8. Burton, P.R. *et al.* Association scan of 14,500 nonsynonymous SNPs in four diseases identifies autoimmunity variants. *Nat. Genet.* **39**, 1329–1337 (2007).
9. Duerr, R.H. *et al.* A genome-wide association study identifies *IL23R* as an inflammatory bowel disease gene. *Science* **314**, 1461–1463 (2006).

10. Becker, C. *et al.* Constitutive p40 promoter activation and IL-23 production in the terminal ileum mediated by dendritic cells. *J. Clin. Invest.* **112**, 693–706 (2003).
11. Mielants, H. *et al.* The evolution of spondyloarthropathies in relation to gut histology. III. Relation between gut and joint. *J. Rheumatol.* **22**, 2279–2284 (1995).
12. Colbert, R.A., DeLay, M.L., Klenk, E.I. & Layh-Schmitt, G. From HLA-B27 to spondyloarthritis: a journey through the ER. *Immunol. Rev.* **233**, 181–202 (2010).
13. Goodall, J.C. *et al.* Endoplasmic reticulum stress-induced transcription factor, CHOP, is crucial for dendritic cell IL-23 expression. *Proc. Natl. Acad. Sci. USA* **107**, 17698–17703 (2010).
14. Mei, Y. *et al.* Increased serum IL-17 and IL-23 in the patient with ankylosing spondylitis. *Clin. Rheumatol.* **30**, 269–273 (2011).
15. Ciccia, F. *et al.* Overexpression of interleukin-23, but not interleukin-17, as an immunologic signature of subclinical intestinal inflammation in ankylosing spondylitis. *Arthritis Rheum.* **60**, 955–965 (2009).
16. Wang, X., Lin, Z., Wei, Q., Jiang, Y. & Gu, J. Expression of IL-23 and IL-17 and effect of IL-23 on IL-17 production in ankylosing spondylitis. *Rheumatol. Int.* **29**, 1343–1347 (2009).
17. Melis, L. *et al.* Systemic levels of IL-23 are strongly associated with disease activity in rheumatoid arthritis but not spondyloarthritis. *Ann. Rheum. Dis.* **69**, 618–623 (2010).
18. Cua, D.J. & Tato, C.M. Innate IL-17–producing cells: the sentinels of the immune system. *Nat. Rev. Immunol.* **10**, 479–489 (2010).
19. Appel, H. *et al.* Immunohistologic analysis of zygapophyseal joints in patients with ankylosing spondylitis. *Arthritis Rheum.* **54**, 2845–2851 (2006).
20. Appel, H. *et al.* Correlation of histopathological findings and magnetic resonance imaging in the spine of patients with ankylosing spondylitis. *Arthritis Res. Ther.* **8**, R143 (2006).
21. Kruithof, E. *et al.* Synovial histopathology of psoriatic arthritis, both oligo- and polyarticular, resembles spondyloarthropathy more than it does rheumatoid arthritis. *Arthritis Res. Ther.* **7**, R569–R580 (2005).
22. McGonagle, D. *et al.* Histological assessment of the early enthesitis lesion in spondyloarthropathy. *Ann. Rheum. Dis.* **61**, 534–537 (2002).
23. Bollow, M. *et al.* Quantitative analyses of sacroiliac biopsies in spondyloarthropathies: T cells and macrophages predominate in early and active sacroiliitis- cellularity correlates with the degree of enhancement detected by magnetic resonance imaging. *Ann. Rheum. Dis.* **59**, 135–140 (2000).
24. Fukuta, S., Oyama, M., Kavalkovich, K., Fu, F.H. & Niyibizi, C., Identification of types II. IX and X collagens at the insertion site of the bovine achilles tendon. *Matrix Biol.* **17**, 65–73 (1998).
25. Gao, J., Messner, K., Ralphs, J.R. & Benjamin, M. An immunohistochemical study of enthesis development in the medial collateral ligament of the rat knee joint. *Anat. Embryol. (Berl.)* **194**, 399–406 (1996).
26. Niyibizi, C., Sagarrigo Visconti, C., Gibson, G. & Kavalkovich, K. Identification and immunolocalization of type X collagen at the ligament-bone interface. *Biochem. Biophys. Res. Commun.* **222**, 584–589 (1996).
27. Sagarriga Visconti, C., Kavalkovich, K., Wu, J. & Niyibizi, C. Biochemical analysis of collagens at the ligament-bone interface reveals presence of cartilage-specific collagens. *Arch. Biochem. Biophys.* **328**, 135–142 (1996).
28. Kumagai, J., Sarkar, K., Uhthoff, H.K., Okawara, Y. & Ooshima, A. Immunohistochemical distribution of type I, II and III collagens in the rabbit supraspinatus tendon insertion. *J. Anat.* **185**, 279–284 (1994).
29. Ralphs, J.R. & Benjamin, M. The joint capsule: structure, composition, ageing and disease. *J. Anat.* **184**, 503–509 (1994).
30. Rufai, A., Benjamin, M. & Ralphs, J.R. Development and ageing of phenotypically distinct fibrocartilages associated with the rat Achilles tendon. *Anat. Embryol. (Berl.)* **186**, 611–618 (1992).
31. Ralphs, J.R., Tyers, R.N. & Benjamin, M. Development of functionally distinct fibrocartilages at two sites in the quadriceps tendon of the rat: the suprapatella and the attachment to the patella. *Anat. Embryol. (Berl.)* **185**, 181–187 (1992).
32. Waggett, A.D., Ralphs, J.R., Kwan, A.P., Woodnutt, D. & Benjamin, M. Characterization of collagens and proteoglycans at the insertion of the human Achilles tendon. *Matrix Biol.* **16**, 457–470 (1998).
33. Gillet, P. *et al.* Studies on type II collagen induced arthritis in rats: an experimental model of peripheral and axial ossifying enthesopathy. *J. Rheumatol.* **16**, 721–728 (1989).
34. Benjamin, M. *et al.* Microdamage and altered vascularity at the enthesis-bone interface provides an anatomic explanation for bone involvement in the HLA-B27–associated spondylarthritides and allied disorders. *Arthritis Rheum.* **56**, 224–233 (2007).
35. Wiekowski, M.T. *et al.* Ubiquitous transgenic expression of the IL-23 subunit p19 induces multiorgan inflammation, runting, infertility, and premature death. *J. Immunol.* **166**, 7563–7570 (2001).
36. Chen, Z.Y., He, C.Y., Ehrhardt, A. & Kay, M.A. Minicircle DNA vectors devoid of bacterial DNA result in persistent and high-level transgene expression *in vivo*. *Mol. Ther.* **8**, 495–500 (2003).
37. Palazzi, C., Salvarani, C., D'Angelo, S. & Olivieri, I. Aortitis and periaortitis in ankylosing spondylitis. *Joint Bone Spine* **78**, 451–455 (2011).
38. Ivanov, I.I. *et al.* The orphan nuclear receptor RORγt directs the differentiation program of proinflammatory IL-17$^+$ T helper cells. *Cell* **126**, 1121–1133 (2006).
39. Grateau, G. & Duruoz, M.T. Autoinflammatory conditions: when to suspect? How to treat? *Best Pract. Res. Clin. Rheumatol.* **24**, 401–411 (2010).
40. May, E. *et al.* CD8 αβ T cells are not essential to the pathogenesis of arthritis or colitis in HLA-B27 transgenic rats. *J. Immunol.* **170**, 1099–1105 (2003).
41. Taurog, J.D. *et al.* Spondylarthritis in HLA-B27/human β2-microglobulin-transgenic rats is not prevented by lack of CD8. *Arthritis Rheum.* **60**, 1977–1984 (2009).
42. McGonagle, D. *et al.* Characteristic magnetic resonance imaging entheseal changes of knee synovitis in spondylarthropathy. *Arthritis Rheum.* **41**, 694–700 (1998).
43. Rahman, P. *et al.* Association of interleukin-23 receptor variants with ankylosing spondylitis. *Arthritis Rheum.* **58**, 1020–1025 (2008).
44. Alonzo, E.S. & Sant'Angelo, D.B. Development of PLZF-expressing innate T cells. *Curr. Opin. Immunol.* **23**, 220–227 (2011).
45. Wofsy, D., Hardy, R.R. & Seaman, W.E. The proliferating cells in autoimmune MRL/lpr mice lack L3T4, an antigen on "helper" T cells that is involved in the response to class II major histocompatibility antigens. *J. Immunol.* **132**, 2686–2689 (1984).
46. Riol-Blanco, L. *et al.* IL-23 receptor regulates unconventional IL-17-producing T cells that control bacterial infections. *J. Immunol.* **184**, 1710–1720 (2010).
47. Cowley, S.C., Meierovics, A.I., Frelinger, J.A., Iwakura, Y. & Elkins, K.L. Lung CD4$^-$CD8$^-$ double-negative T cells are prominent producers of IL-17A and IFN-γ during primary respiratory murine infection with *Francisella tularensis* live vaccine strain. *J. Immunol.* **184**, 5791–5801 (2010).
48. Crispín, J.C. *et al.* Expanded double negative T cells in patients with systemic lupus erythematosus produce IL-17 and infiltrate the kidneys. *J. Immunol.* **181**, 8761–8766 (2008).
49. Ling, E., Shubinsky, G. & Press, J. Increased proportion of CD3$^+$CD4$^-$CD8$^-$ double-negative T cells in peripheral blood of children with Behcet's disease. *Autoimmun. Rev.* **6**, 237–240 (2007).
50. Venzor, J., Hua, Q., Bressler, R.B., Miranda, C.H. & Huston, D.P. Behcet's-like syndrome associated with idiopathic CD4$^+$ T-lymphocytopenia, opportunistic infections, and a large population of TCRαβ$^+$ CD4$^-$ CD8$^-$ T cells. *Am. J. Med. Sci.* **313**, 236–238 (1997).
51. Sakamoto, A. *et al.* T cell receptor Vβ repertoire of double-negative α/β T cells in patients with systemic sclerosis. *Arthritis Rheum.* **35**, 944–948 (1992).

## ONLINE METHODS

**Mice.** B10.RIII and C57BL/6 mice were obtained from Jackson Laboratories, and C57BL/6 *Rag2*$^{-/-}$ mice were obtained from Taconic Farms. IL-23R–eGFP mice[52] and ROR-γt–eGFP C57BL/6 mice[53] were bred with B10.RIII mice to generate experimental F1 GFP reporter mice for use. All mice used were male. B10.RIII mice were used for minicircle expression unless otherwise stated. All animal procedures were approved by the Institutional Animal Care and Use Committee of Merck, Palo Alto, in accordance with guidelines of the Association for Assessment and Accreditation of Laboratory Animal Care.

**Histology.** Formalin-fixed tissue was decalcified in ImmunoCal (Decal Chemical Corp) and paraffin embedded. Enthesitis was scored for using the following factors: extent and severity of enthesitis, bony proliferation and lysis and joint space involvement. Osteoblasts were visualized with the SigmaFast Red TR/Naphthol AS-MX Kit, and osteoclasts were visualized using the K-ASSAY TRAP staining kit (Kamiya Biomedical). For immunohistochemistry, we used antibodies to the following: Ki-67 (TEC-3, Dako, 37 μg/ml), F4/80 (BM8, eBioscience, 1.25 μg/ml), MPO (A0398, Dako, 1.65 μg/ml) or CD3 (A0452, Dako, 3 μg/ml), with DAB chromogen (Dako).

**Flow cytometry.** Antibodies to the following were obtained from BD Biosciences: CD4 (RM4-5), CD3 (145-2C11), CD8 (53-6.7), IL-17A (TC11-18H10), NK1.1 (PK136), NKp46 (29A1.4) and B220 (RA3-6B2). Antibodies to the following were from eBioscience: IL-22 (1-H8PWSR), Thy1.2 (30-H12), CD45 (30-F11) and Sca1 (D7). Unconjugated antibody to CD16/32 (2.4G2, Merck) was used. Antibody to chemokine (C-C motif) receptor 6 (CCR6) (29-2L17) was from BioLegend. Antibodies were used at a 1:100 dilution, except for antibodies to IL-17A and IL-22, which were used at a 1:50 dilution. CD1d tetramers were from ProImmune and were used at a 1:200 dilution. A Canto II flow cytometer (BD Biosciences) and FlowJo FACS software were used for analysis, and a FACS Aria II (BD Biosciences) was used for cell sorting.

**Collagen-antibody–induced disease.** Male B10.RIII mice received 2 mg of antibody to type II collagen (Chondrex) i.v. on day 0 with 1 mg of antibody to IL-23p19 (Merck) or IgG1 isotype control. Clinical score was graded per paw as follows: 0, normal; 1, swelling of one digit; 2, swelling of two or more digits; or 3, swelling of the entire paw. Scores were added to produce a final score.

**Molecular profiling of paw gene expression.** Tissues were homogenized in RNA STAT-60 (Tel-Test), and the RNA was precipitated in isopropanol, re-extracted with phenol, chloroform and isoamyl alcohol and cleaned using the QIAGEN RNeasy mini RNA cleanup protocol (QIAGEN). DNase-treated total RNA was reverse transcribed using QuantiTect Reverse Transcription (QIAGEN). Primers were designed using Primer Express (Applied Biosystems, Life Technologies, Foster City, CA) or obtained from Applied Biosystems. Real-time PCR was performed using either an Applied Biosystems SYBR Green assay or a FAM-labeled probe (Applied Biosystems) in a TaqMan real-time quantitative PCR reaction with an ABI 7300 sequence detection system. Data was normalized to ubiquitin by the ΔΔCt method.

**Molecular profiling of entheseal resident cells.** Twenty to thirty cells were sorted into a CellsDirect One-Step qRT-PCR kit (Life Technologies). Samples were pre-amped for 18 cycles, and real-time PCR was performed on a Fluidigm Biomark system.

**Multiphoton microscopy.** The heal or axial skeleton was maintained in an oxygenated Aqix RS-I solution (Aqix), and images were collected on a Leica SP5X coupled with a Coherent Chameleon Ultra II Ti:Sapphire multiphoton laser.

**Entheseal cell isolation.** Mice were perfused, their skin was removed, and their extensor and Achilles' tendons were traced to the point of insertion. A 2-mm length of tissue was taken by cutting the tendon insertion at the surface of the bone, avoiding bone or bone marrow, and digested in DMEM containing 5% FCS (Hyclone) and 5 mg/ml type 2 collagenase (Worthington). For intracellular staining, cells were fixed in 2% paraformaldehyde and permeabilized with PermWash (BD Pharmingen).

**Entheseal histoculture.** The Achilles' entheses isolated as described above were cultured overnight on filters (PICM0RG50, Millipore) in complete Iscove's Modified Dulbecco's Medium (IMDM) with IL-6 (100 ng/ml), TNF (7.5 ng/ml) (both R&D) or IL-23 (10 ng/ml) (Merck).

***In vivo* antibody administration.** Antibody to CD4 (GK1.5, Merck) was administered subcutaneously 1 d before administration of IL-23mc and weekly thereafter. Antibodies to TNF (XT22, Merck), IL-6 (20F3, Merck), RANKL (IK22/5, BioXCell), IL-17 (1D10, Merck) and IL-22 (142928, R&D) were administered subcutaneously at day 5 after IL-23mc administration and weekly thereafter. All antibodies were used at a dose of 30 mg/kg.

**Minicircle vector construction.** The linked IL-23 p40-p19 DNA or other cytokine DNAs were cloned into the p2øC31.RSV.hAAT.bpA minicircle-producing plasmid provided by Z.-Y. Chen (Departments of Pediatrics and Genetics, Stanford University School of Medicine), using standard molecular techniques. Minicircle DNA was produced following the methods described by Chen *et al.*[54] with minor modifications and was injected intravenously in Ringer's solution at a total volume of 10% of the weight of the mouse.

**Analysis of effects of IL-22 on bone.** Frozen optimal cutting temperature medium (OCT)-embedded paw sections were stained with DAPI (Vector) and pSTAT3 (4/P-STAT3, Cell Signaling) with detection by antibodies to rabbit IgG. Northern Lights (493, Cell Signaling). The osteoblast cell line CRL-12424 was stimulated for 15 min with 100 ng/ml of IL-6 or IL-22 (both R&D). Cells were stained for vascular cell adhesion molecule (VCAM) (429, BD).

**Serum cytokine quantification.** IL-23 was measured using streptavidin-coated 96-well plates (Meso Scale Discovery), with capture anti-mouse IL-23p19 (R&D) and sulfo-tagged rat antibody detecting mouse IL-23p40 (Merck).

**Bone computed tomography.** Hind paws were scanned with a GE eXplore Lotus scanner (GE Healthcare) on excised paws. Three-dimensional image rendering was generated using Microview software (GE Healthcare).

**Statistics.** Statistical tests were carried out using GraphPad Prism 5 software. A Student's *t* test was used for parametric data, and the Mann-Whitney test was used for non-parametric data. Heatmaps were generated using Spotfire software (TIBCO).


52. Awasthi, A. *et al.* Cutting edge: IL-23 receptor gfp reporter mice reveal distinct populations of IL-17-producing cells. *J. Immunol.* **182**, 5904–5908 (2009).
53. Lochner, M. *et al. In vivo* equilibrium of proinflammatory IL-17$^{+}$ and regulatory IL-10$^{+}$ Foxp3$^{+}$ RORγt$^{+}$ T cells. *J. Exp. Med.* **205**, 1381–1393 (2008).
54. Chen, Z.Y., He, C.Y. & Kay, M.A. Improved production and purification of minicircle DNA vector free of plasmid bacterial sequences and capable of persistent transgene expression *in vivo*. *Hum. Gene Ther.* **16**, 126–131 (2005).